ChemComm

FEATURE ARTICLE

Open Access Article. Published on 14 June 2023. Downloaded on 1/14/2025 4:37:19 PM. This article is licensed under a Creative Commons Attribution-NonCommercial 3.0 Unported Licence.

Cite this: *Chem. Commun.*, 2023, **59**, 8375

Received 3rd April 2023,
Accepted 2nd June 2023

DOI: 10.1039/d3cc01634j

rsc.li/chemcomm

Exploring innovative designs and heterojunctions in photocatalytic micromotors

Katherine Villa

Photocatalytic micromotors that convert light energy into mechanical energy have garnered increased interest due to their fast photoactivation, and potential for precise control and manipulation. This feature article provides key insights into the design of photocatalytic micromotors by using single semiconductors, and heterostructures. It also highlights the different strategies to develop efficient light-driven micromotors by minimizing electron–hole pair recombination and improving charge transfer among components. The remaining challenges and possible solutions are also discussed.

Introduction

Photoactive micromotors, made of semiconducting components, are a type of microscale device that can convert light energy into mechanical energy through photocatalytic reactions. Over the last few years, there has been an increased interest in these types of micromotors, due to their multi-wavelength light responses, chemical stability, and ability to harvest both chemical and light energy to induce self-propulsion.[1,2]

The photocatalytic material, usually an inorganic or organic semiconductor, absorbs light and generates electron–hole pairs. These charge carriers can then react with water or other chemicals in the environment, creating a gradient that propels the micromotor forward by different phoretic mechanisms.[1] A more detailed explanation of the motion mechanisms can be found in previous reviews.[1–3] By controlling the intensity, polarization, wavelength, and direction of the light, researchers can manipulate the motion of these devices, making them useful for a range of applications in fields such as biomedical engineering,[3] environmental remediation, and energy harvesting. Moreover, the concentration and type of chemicals present in the liquid media can also influence their motion behaviors.

The robustness and variety of semiconductors make them ideal candidates for designing light-driven micromotors in comparison to photoactive organic compounds, such as azobenzene, that exhibit restricted light activation to specific wavelengths.[4] Moreover, semiconductor-based micromotors offer the possibility of light absorption modulation by choosing materials with suitable bandgaps. Based on the position of the conduction and valence band potentials of the semiconducting components, the oxidative and reductive properties of these micromotors can be modulated as well. Therefore, light-driven photocatalytic micromotors with tuneable redox capabilities can be designed for specific target reactions.

The chassis of photocatalytic micromotors can be fabricated in various shapes and sizes, including spheres,[5] rods,[6] tubes,[7] flowers,[8] stars,[9] butterfly-like,[10] or more complex structures,[11,12] to achieve specific movement patterns. Photocatalytic micromotors are typically composed of titanium dioxide. While this material has proven useful, its optical absorption limited to the UV range has led to the development of alternative micromotors composed of semiconductors that respond to visible and/or near-infrared wavelengths. In recent years, significant progress

Institute of Chemical Research of Catalonia (ICIQ), The Barcelona Institute of Science and Technology (BIST), Av. Països Catalans, 16, Tarragona E-43007, Spain. E-mail: kvilla@iciq.es

Katherine Villa

Katherine Villa received her PhD degree in Chemistry from the Autonomous University of Barcelona, Spain. After two research positions at the Catalonia Energy Research Institute and the Institute for Bioengineering of Catalonia, she joined the Center for Advanced Functional Nanorobots at the University of Chemistry and Technology, Prague (Czech Republic), where she worked as a senior scientist for 3 years. Currently, she is leading a research group on light-driven nanomotors and solar fuels at the Institute of Chemical Research of Catalonia (ICIQ). Her research interests include photocatalysis, micro/nanomotors, nanomaterials, renewable energy, and environmental remediation.

Open Access Article. Published on 14 June 2023. Downloaded on 1/14/2025 4:37:19 PM.
This article is licensed under a Creative Commons Attribution-NonCommercial 3.0 Unported Licence.

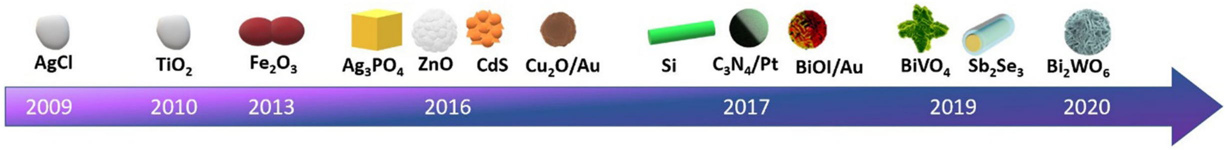

Fig. 1 Evolution of the design of photocatalytic micromotors from UV to visible-light responsive materials with different morphologies over the last years.

has been made in this field, resulting in the creation of more advanced and versatile light-driven micromotors.[6,7,9,13,14]

Since the pioneering works on amorphous AgCl and TiO_2 micromotors by Sen and co-authors,[15,16] a quite broad range of photocatalytic micromotors have been further designed, involving either single-component and/or multicomponent heterostructures. As can be seen in Fig. 1, the first examples of photocatalytic micromotors included UV-light responsive materials, in which the asymmetry required for their autonomous motion was provided by a heterogeneous rough surface. Then, more defined structures consisting of visible light-responsive photocatalysts were fabricated, including Fe_2O_3,[17] CdS,[18] and Ag_3PO_4.[18] To enhance the electron–hole pair separation, Janus particles with metal–semiconductor heterostructures were further reported, including C_3N_4/Pt,[19] Cu_2O/Au,[13] and BiOI/Au.[20] The use of photocatalysts with hybridized orbitals and short bandgaps,[9,21] such as $BiVO_4$, also represented a promising strategy to design efficient visible-light-driven photocatalytic micromotors with enhanced speeds and improved motion capabilities, even in highly viscous glycerol media.[9] Alternatively, the fabrication of heterostructured micromotors based on p–n junctions is also an attractive way of developing more sophisticated photoactive micromotors without the need of using noble metals. By focusing on the material properties, fabrication, and rational design of semiconductor structures, more efficient and robust photocatalytic micromotors can be developed in the future. Therefore, these different configurations along with their advantages and disadvantages are described in the following sections.

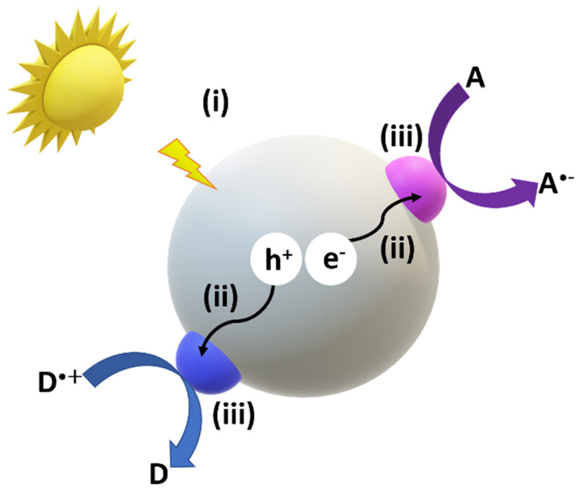

Fig. 2 Photocatalytic mechanism illustrating the different steps that take place on a photocatalytic micro/nanomotor upon irradiation.

Photocatalytic principles

The photoactivation of a semiconductor involves a series of processes that are influenced by the optical and morphological properties of the photocatalysts as well as the nature of the solid–liquid interfaces. The threshold wavelength required for inducing photocatalytic reactions can be estimated from the bandgap energy of the material (E_{gap}), as shown in eqn (1). Where h corresponds to the Planck's constant (6.63×10^{-34} J s) and c is the speed of light (3.00×10^8 ms^{-1}) and E_{gap} is expressed in eV.[22] Therefore, wide-bandgap semiconductors are commonly used to develop UV-light responsive micromotors, while intermediate and short-bandgap semiconductors are often used to design micromotors with light absorption in the visible and near-infrared, respectively.

$$\lambda(\mathrm{nm}) = \frac{hc}{E_{gap}} = \frac{1240}{E_{gap}} \quad (1)$$

As represented in Fig. 2, the main steps of the photoactivation of the micromotors includes photon absorption (i), electron–hole pair separation (ii), diffusion and transport of the photogenerated charge carriers (ii), reaction efficiency, and mass transfer of reactants and products (iii).[23] All the above factors have a direct influence on the self-propulsion capabilities of photocatalytic micromotors. Usually, generation, trapping, and recombination of the photogenerated charges occur in the femto-, pico-, and nano-seconds, while interfacial surface reactions take place at milli-second time scales.[24] Therefore, the electron–hole pair recombination rates limit the overall photocatalytic motion efficiencies and is the bottleneck of photocatalytic processes. To overcome this limitation and enhance photocatalytic efficiencies, researchers have explored various strategies, *e.g.*, incorporating noble metals and/or dual semiconductor components within the same structure of the micromotors. These approaches have been extensively investigated in recent years and show promise in improving the overall photocatalytic performance. In the following sections, we will discuss the most representative examples of current designs of photocatalytic micromotors. A summary of such works is also included in Table 1.

Single component micromotors

Single component photocatalytic micromotors have the advantage of requiring simple fabrication techniques based on wet chemical methods, such as hydrothermal, sol–gel, and co-precipitation reactions. Moreover, the yield of micromotors is usually higher than the obtained by large equipment, *e.g.*,

Open Access Article. Published on 14 June 2023. Downloaded on 1/14/2025 4:37:19 PM. This article is licensed under a Creative Commons Attribution-NonCommercial 3.0 Unported Licence.

Table 1 Representative examples of photocatalytic micromotors based on single component and heterostructures, including metal–semiconductor and semiconductor–semiconductor junctions

Type of micromotor	Material	Light source	Fuel type (% wt)	Motion mechanism	Size (μm)	Speed (μm s^{-1})	Fabrication method	Ref.
Single semiconductor	AgCl	UV	Water	Self-diffusiophoresis	1	100	Co-precipitation	15
Single semiconductor	TiO_2	UV	Water	Self-diffusiophoresis	0.2–2.5	10	Commercial particles	16
Single semiconductor	Fe_2O_3	Visible	H_2O_2 (1)	Self-diffusiophoresis	1.5	4.5	Sol–gel	17
Single semiconductor	$BiVO_4$	Visible	H_2O_2 (0.025)	Self-diffusiophoresis	4–8	5	Hydrothermal	9
Single semiconductor	Bi_2WO_6	Visible	Water	Self-diffusiophoresis	7	1.9	Hydrothermal	21
Single semiconductor	C_3N_4	Visible	H_2O_2 (30)	Bubble-recoil	67	72	Hydrothermal	7
Metal–semiconductor	Cu_2O/Au	Visible	H_2O_2 (3)	Self-electrophoresis	1.2	6	Co-precipitation/thermal evaporator	13
Metal–semiconductor	TiO_2/Au	UV	Water	Self-electrophoresis	1	25	Solvent extraction/evaporation/sputtering	5
Metal–semiconductor	C_3N_4/Pt	UV	Water	Self-electrophoresis	2.6	23	Calcination/metal reduction	19
Metal–semiconductor	BiOI/Au	Visible	Water	Self-electrophoresis	2–4	1.62	Self-assembly/sputtering	20
Metal–semiconductor	Si/Au	Visible	Water	Self-electrophoresis	4	5	Glancing angle deposition/thermal evaporator	36
Semiconductor–semiconductor	TiO_2/Cu_2O	UV and visible	H_2O_2 (1.5)	Self-phoresis/osmotic flow	4–5	—	Drop casting/thermal evaporator	12
Semiconductor–semiconductor	TiO_2/CoO	UV and Visible	Water	Self-electrophoresis	2–6	11.5 (visible) and 6.5 (UV)	Drop casting/sputtering	48
Semiconductor–semiconductor	p-Si/n$^+$-Si	Visible	H_2O_2 (0.5)	Self-electrophoresis	15	38	Metal-assisted electroless chemical etching/photolithography/sputtering	6
Semiconductor–semiconductor	Si/TiO_2	UV	H_2O_2 (0.1)	Self-electrophoresis	11	6	wet etching/atomic layer deposition/hydrothermal	11
Semiconductor–semiconductor	Sb_2S_3/ZnO	Visible	1,4-Benzoquinone/hydroquinone	Self-electrophoresis	10	12	Atomic layer deposition	49
Semiconductor–semiconductor	GaN/ZnO/Au	UV	H_2O_2 (10)	Self-diffusiophoresis	4.6	5.5	Epitaxial growth/sputtering	51
Semiconductor–semiconductor	TiO_2/CdS	UV and visible	Water	Self-electrophoresis	8	11.3	Hydrothermal/ion-exchange/atomic layer deposition	54

physical vapor deposition or sputtering techniques.[25] The first examples of photocatalytic micromotors based on a single material consisted of UV-light responsive materials such as AgCl and TiO_2, that were either unstable[15] or required high concentrations of chemical fuels.[16] Such drawbacks, combined with the necessity for a light source that was more biocompatible, have prompted the development of micromotors that respond to visible light. Therefore, semiconductors with a bandgap ranging from 2.1–2.8 eV are commonly employed as the chassis of visible-light-driven photocatalytic micromotors. Some of the most representative examples of single component photocatalytic micromotors, include the design of peanut-shaped hematite micromotors with a size of about 1.5 μm length and ∼0.6 μm diameter.[17] Upon blue light irradiation, these micromotors self-propel along the surface in the presence of H_2O_2 as chemical fuel and tetramethylammonium hydroxide. Taking advantage of their magnetic responses, the motion direction was externally controlled by a weak magnetic field (∼1 mT). In addition, the direction was also steered by using a patterned surface. Moreover, the authors found that the etching of the surface of the micromotors was key to enhance their motion capabilities, due to an enhanced surface anisotropy. By increasing the pH of the solution, these micromotors were able to perform capture and cargo transportation of particles of sizes up to 20 μm with the aid of magnetic fields (Fig. 3(A)).[17] This work illustrates the versatility that photocatalytic micromotors offer for motion control and manipulation.

The development of totally metal-free C_3N_4 tubular micromotors that were prepared by a template-less method also represented an important milestone towards scalable fabrication methods for their potential application in the environmental field.[7] This material possesses unique electronic and optical properties, making it an attractive candidate for various applications, ranging from biomedicine[26] to environmental remediation. In the latter, it was found that C_3N_4 micromotors were able to capture different heavy metals present in the solution.[7] This was attributed to metal complex formation and/or acid–base interactions between the surface of the micromotors and the metals. As a result, the speed of the micromotors increased up to 30%, requiring 20 times less amount of fuel for propulsion. On the other hand, owing to their intrinsic fluorescence, it was also possible to get an insight into the heavy metal removal rates by fluorescence quenching. Furthermore, taking advantage of their big sizes, it was possible to visualize the bubble formation rates (12–13 ms) and ejection (88 ms) over time. Overall, this study showed the opportunities that photocatalytic micromotors offer for pollutant removal with the concomitant visualization of such a decontamination process by optical means.

On the other hand, C_3N_4-derivates can store light energy by electron storage-release mechanisms and drive the motion of photoactive micromotors in the absence of light.[27] Although this property is limited to this kind of materials and depends on the conditions of the liquid media, it is an interesting

Open Access Article. Published on 14 June 2023. Downloaded on 1/14/2025 4:37:19 PM.
This article is licensed under a Creative Commons Attribution-NonCommercial 3.0 Unported Licence.

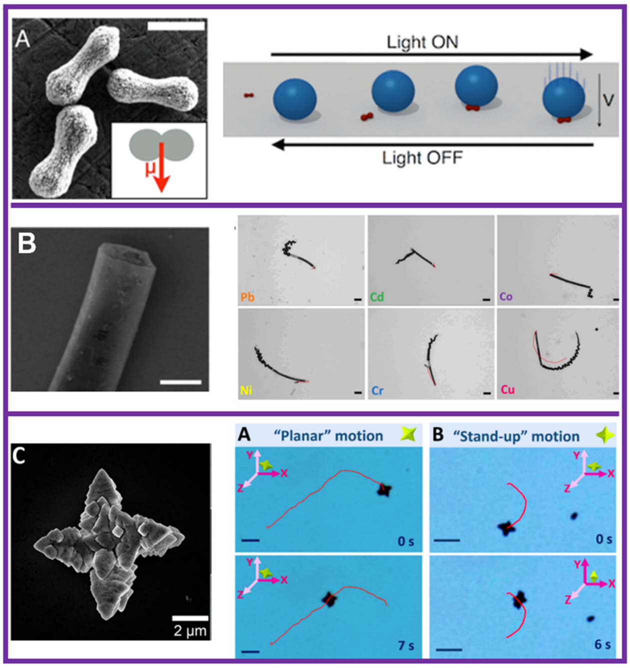

Fig. 3 Most representative examples of single-component micromotors that are based on visible-light-responsive materials. (A) Hematite peanut-shaped micromotors for cargo transportation. Adapted with permission from ref. 17. Copyright 2013, American Chemical Society. (B) Metal-free C_3N_4 tubular micromotors for the removal of heavy metals. Adapted with permission from ref. 7. Copyright 2018, American Chemical Society. (C) Star-shaped $BiVO_4$ micromotors for removal of microbial contamination. Adapted with permission from ref. 9. Copyright 2019, American Chemical Society.

approach to further expand the applicability of these devices in highly scattering environments.

The introduction of star-shaped $BiVO_4$ micromotors consolidated this material as a benchmark photocatalysts for fabricating visible-light responsive micromotors with a high efficiency and photostability. By changing the morphology from single-star to twin-star shaped, it was possible to modulate their motion capabilities from planar to stand-up motion modes.[9] Moreover, these $BiVO_4$ micromotors also showed smart features such as the autonomous ability to change their motion trajectories to capture and transport yeast cells. It should be noted that no magnetic guidance or surface modification was carried out. Moreover, the same yeast seeking behaviour was also confirmed in the presence of other microorganisms, such as *E. coli*. Further works have applied $BiVO_4$ micromotors for preventing microbial contamination in alcoholic beverages,[28] oxidation of benzylamine,[29] as well as degradation of organic pollutants.[10]

To sum up, single component micromotors offer several advantages in terms of fabrication and high mass-production, allowing for large-scale manufacturing. Moreover, these micromotors can be produced using low-cost fabrication techniques,[30] making them economically viable for various applications. Another advantage is the simplicity of their synthesis process, typically involving a one-step procedure. However, these type of micromotors often require the addition of chemical fuels for their propulsion, which can limit their autonomy and introduce additional complexity. Furthermore, their light absorption capability is usually limited to a specific wavelength region, which restricts their performance in broader light spectra. These types of micromotors usually suffer from high recombination rates of photogenerated electron–hole pairs, limiting their overall efficiency. To address some of these limitations, potential strategies such as crystal faceting show promise in enhancing the photoactivity of single component micromotors.[31,32] Such configuration promotes electron–hole separation in each crystal facet within the same material, leading to enhanced motion efficiencies and photocatalytic performances.

Metal–semiconductor heterojunction

A metal–semiconductor interface is the junction between both materials. This interface has important properties for electronic devices and photovoltaic applications, as it can act as a barrier to the flow of electrical charge carriers or as a means of creating a junction for electronic devices. An optimal contact between the semiconductor and the metal is given by the characteristics of the materials and the type of contact formed between the metal and the semiconductor. Usually, ohmic junctions are formed with highly doped semiconductors, while Schottky junctions are established with slightly doped semiconductors.[33] Fig. 4 represents the band alignment of a metal–semiconductor (n-type) before and after contact. The vacuum level, denoted as E_0, is the energy state of electrons with zero kinetic energy outside the material, either metal or semiconductor. The Fermi energy (E_F) represents the highest occupied electron energy state at $T = 0$ K in a metal; in a non-degenerate semiconductor it lies in the gap between the valence and the conduction band. The energy difference between the Fermi energy and the vacuum level is defined as the work function, represented by Φ. On the other hand, the electron affinity, represented by χ, is defined as the energy required to move an electron from the vacuum level to the conduction band. Upon contact, the differences in the work functions lead to electron transfer from the semiconductor to the metal until the respective Fermi levels align at equilibrium. This results in the formation of a depletion region in the semiconductor, where W is the width of such a region and Φ_B is the height of the potential barrier that an electron in the metal must overcome to move into the semiconductor.[34]

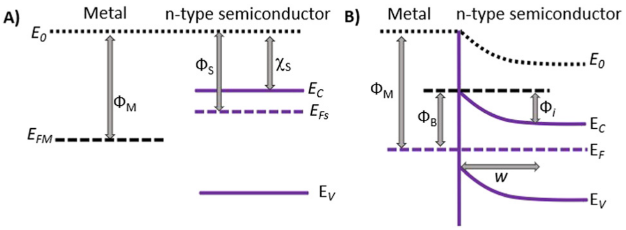

Fig. 4 Schematic representation of the energy levels of a metal–semiconductor interface before (A) and after contact (B).

Open Access Article. Published on 14 June 2023. Downloaded on 1/14/2025 4:37:19 PM.
This article is licensed under a Creative Commons Attribution-NonCommercial 3.0 Unported Licence.

The design of metal–semiconductor junctions is then a common strategy for minimizing electron–hole pair recombination. Usually, the decoration of semiconductors with co-catalysts, such as Pt and RuO_2, leads to an enhancement of the reductive and oxidative pathways, respectively. In the field of photocatalytic micro/nanomotors, the design of Janus photocatalytic micromotors based on a metal–semiconductor heterojunction has been widely explored. One of the main advantages of these type of heterostructures in comparison with single-component semiconductors is their ability to achieve fast speeds in pure water. The first study based on this configuration included TiO_2/Au micromotors that showed a high motion efficiency in pure water.[5] The same heterostructure was also further applied to nanomotors, showing propulsion abilities in water as well.[35] After this pioneering work, other type of Janus metal–semiconductor micromotors based on UV or visible-light responsive photocatalysts were further reported, including Cu_2O/Au,[13] Si/Au,[36] Fe_2O_3/Au,[37] BiOI/Au,[20] ZnO/Pt,[8] C_3N_4/Pt,[19] and AgCl/Ag.[38] However, some of these micromotors still require the addition of chemical fuels, such as H_2O_2 or organic solvents, to exhibit stronger propulsion abilities.

To illustrate the effect of the metal work function on the performance of photocatalytic micromotors, we considered Janus TiO_2 micromotors as an example. As shown in Fig. 5(A), various Janus TiO_2 micromotors with a spherical shape and containing different metallic counterparts have been reported, including TiO_2/Pt,[39] TiO_2/Au,[5] TiO_2/Cu,[40] TiO_2/PtPd[41] and TiO_2/Fe.[42] The differences between the metal work function values and the electron affinity of the semiconductor affect the formation of the resulting Schottky barrier, which has a direct influence on their motion capabilities (Fig. 5(B)).[43] The reported velocities for Janus TiO_2 micromotors based on Pt, Au, Cu, and Fe micromotors are 26.2, 25, 22.8, and 1.96 body length s^{-1}, respectively. Therefore, the larger the work function difference with respect to the semiconductor, the higher the motion speeds. This can be attributed to the Schottky barrier junction, where the metallic counterpart acts as an electron sink and reduction active site. This contributes to minimize electron–hole pair recombination, increasing the overall photocatalytic performance. Thus, the work function value is an important parameter to consider when designing Janus micromotors based on metal–semiconductor junctions.

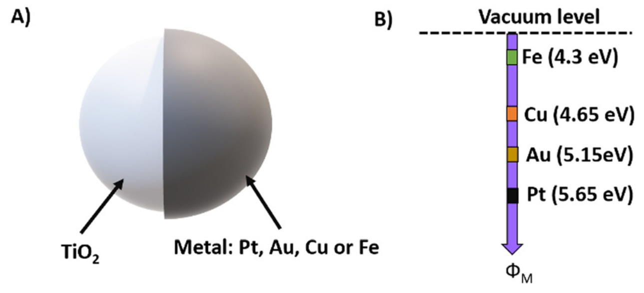

Fig. 5 Janus photocatalytic TiO_2 micromotors. (A) Schematic representation showing the different examples of Janus TiO_2/metal micromotors. (B) Metal work functions of Fe, Cu, Au, and Pt.

An additional advantage of Janus micromotors in comparison to single component micromotors is their ability to self-propel at a very low light intensity (2.5×10^{-3} W cm^{-2}).[5] Furthermore, as any photoresponsive micromotor, the motion speeds can be increased by modulating the light intensity (Fig. 6(A)–(E)).

An alternative strategy to control the motion of photoactive micromotors is by taking advantage of the light penetration in semiconductors. When a light beam hits a semiconductor material, there is a decrease in the intensity as it traverses through the material. Therefore, the absorption coefficient of a semiconductor estimates how strongly the material absorbs light.[18] For example, in silicon, the absorption coefficient is highest at shorter wavelengths and decreases as the wavelength increases. This means that blue light is absorbed more strongly than red light, and that light of shorter wavelengths can penetrate less deeply into the material than light of longer wavelengths.

Zhang *et al.* fabricated phototactic photocatalytic micromotors based on the limited light penetration depth in isotropic particles, including TiO_2, CdS, and ZnO.[18] By using a home-made experimental setup, it was possible to control the movement direction of the micromotors along *X* and *Y* axes. As can be seen from Fig. 6(F), TiO_2 micromotors followed a predesigned motion trajectory, due to their phototactic behavior and sophisticated light control setup. Such motion control by the external light beam direction was greatly affected by the size of

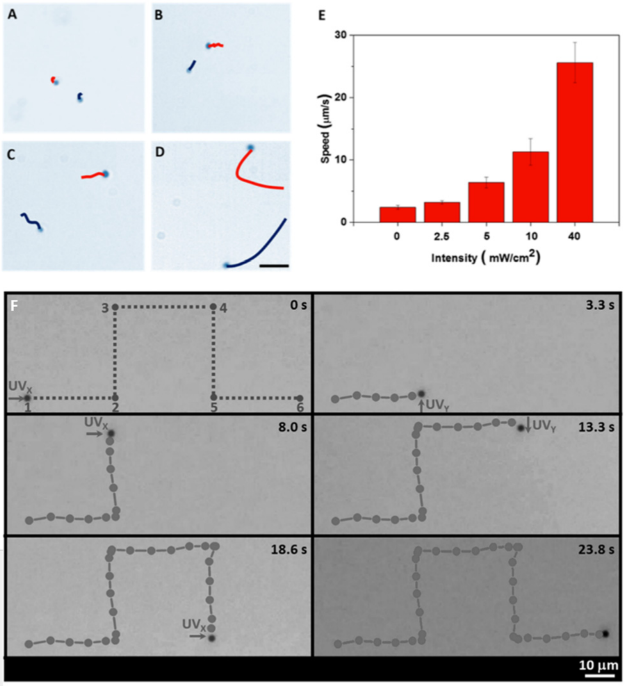

Fig. 6 Light control of photocatalytic micromotors. (A) Motion trajectories and velocities of TiO_2/Au Janus micromotors at different light intensities. Adapted with permission from ref. 5. Copyright 2016, American Chemical Society. (B) Motion control of TiO_2 micromotors along *X* and *Y* light directions. Reproduced from ref. 18 with permission from John Wiley and Sons, copyright 2016.

Open Access Article. Published on 14 June 2023. Downloaded on 1/14/2025 4:37:19 PM.
This article is licensed under a Creative Commons Attribution-NonCommercial 3.0 Unported Licence.

the micromotor. For sizes of about 1 μm, the micromotors showed phototactic behaviors, because the diameter was much larger than the penetration depth (δ). However, this was not observed for micromotors of 0.4 μm diameter since the light penetrated almost the whole body of the micromotor. On the other hand, when the size was increased up to 3.5 μm, the micromotor showed stronger friction with the glass hampering its motion.

Other factors, such as surface area or crystalline structure of the photocatalysts have also an influence on the motion efficiencies of photoactive micromotors. A more detailed discussion can be found in previous reviews.[2,8]

Overall, metal–semiconductor heterojunctions offer several advantages in their design and functionality. One notable advantage is their ability to self-propel in pure water under low light intensities, making them highly versatile for various environments and broadening their range of applications to biocompatible scenarios. Such metal–semiconductor-based micromotors also demonstrate high motion efficiencies and low recombination rates, resulting in improved overall performance. However, there are some disadvantages associated with their fabrication. One drawback is the low micromotor yield, which can limit their scalability and practical implementation. Additionally, the fabrication techniques required for creating these heterojunctions can be expensive and robust, posing challenges in terms of cost and feasibility. Moreover, the multistep fabrication process adds complexity and increases the chances of process-related issues. Potential strategies to overcome these challenges include using low-cost metals such as Fe, Cu, and Ni, or metal alloys, *e.g.*, Cu/Ni and Fe/Ni. Furthermore, exploring alternative fabrication processes like emulsion polymerization, electrostatic assembly, and microfluidic techniques may offer cost-effective and accessible production of metal–semiconductor heterojunctions.

Semiconductor–semiconductor heterojunction

The development of light-driven micromotors by combining two semiconductors in the same structure is also an interesting approach to overcome the main limitations of single semiconductor-based microdevices, *e.g.*, light absorption under specific wavelength region, limited redox potential and fast charge-pair recombination. Heterostructures are often used to facilitate charge transfer between the materials, which is necessary for the generation of a driving force. As shown in Fig. 7, there are two main types of heterostructure junctions: p–n junction and *Z*-scheme. The p–n heterojunction consists of the junction formed between a n-type semiconductor and a p-type semiconductor (Fig. 7(A)).[44,45] Upon photoactivation, the photogenerated electrons from photocatalyst II (PS II) migrate to the conduction band of the photocatalyst I (PS I) to equilibrate the Fermi levels. In a similar fashion, the photogenerated holes from the valence band of PS I are transferred to the valence band of PS II. This results in the formation of an electrical field at the p–n interface that can drive the electrons and holes to migrate in opposite directions.[43] Owing to this electron–hole separation, the charge pair recombination is greatly inhibited and the lifetime of the photogenerated carriers is extended.[44]

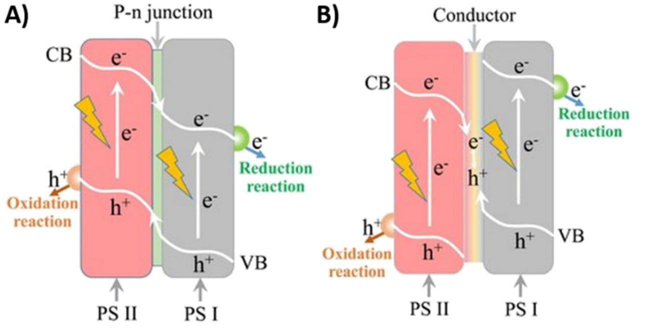

Fig. 7 Schematic illustration of charge transfer in semiconductor heterojunctions. (A) P–n semiconductor junction and (B) Solid-state *Z*-scheme. Reproduced from refs. 44 and 45 with permission from John Wiley and Sons, copyright 2014, and licensee Beilstein-Institut, copyright 2018, respectively.

In contrast to p–n configurations, where the redox potential is reduced compared to the bare semiconductors, the development of an all-solid-state *Z*-scheme heterostructure presents a promising approach to creating a photocatalytic system with a strong redox potential and minimal electron–hole pair recombination. This configuration allows for photogenerated electrons from PS II to combine with photogenerated holes from PS I, facilitated by the formed Ohmic contact (Fig. 7(B)).[44] The resulting electrons, with a more negative potential, can then be utilized to carry out reductive reactions, while the holes, with a more positive potential, can be used for performing oxidative reactions. The formation of this heterostructure junction can be achieved through physical contact or with a solid electron mediator.[46] A very well-known example of this solid *Z*-scheme configuration for the photocatalytic water splitting is the combination of Ru/$SrTiO_3$:Rh and $BiVO_4$.[47] However, this configuration is yet to be explored for the construction of light-driven heterostructured micromotors.

Photocatalytic micromotors based on p–n heterojunctions have shown promising results in recent years. One example is the design of a TiO_2/Cu_2O micromotor, which has a unique chevron shape and is capable of self-propelling in both H_2O_2 and pure water (Fig. 8(A)).[12] By combining materials that respond to both UV and visible light within a single motor structure, it became feasible to adjust the types of motion exhibited by the motor, shifting from translational to rotational, simply by altering the light wavelength from UV to blue. By following a similar approach, it was also possible to control the movement direction of TiO_2/CoO Janus micromotors by switching from UV to visible wavelengths (Fig. 8(B)).[48] In this configuration, TiO_2 is only photoactivated under UV light, while visible light irradiation activates mostly the CoO counterpart. Therefore, the motion direction was changed by changing the electron transfer dynamics among components.

Open Access Article. Published on 14 June 2023. Downloaded on 1/14/2025 4:37:19 PM.
This article is licensed under a Creative Commons Attribution-NonCommercial 3.0 Unported Licence.

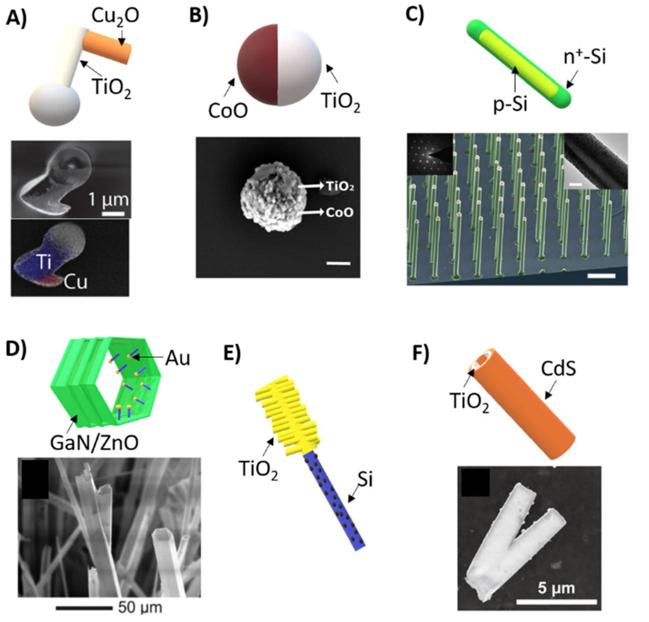

Fig. 8 Photocatalytic micromotors based on semiconductor–semiconductor junctions. (A) TiO_2/Cu_2O micromotors and SEM/EDS images that show their chevron-like morphology and elemental mapping. Reproduced from ref. 12 with permission from John Wiley and Sons, copyright 2018. (B) TiO_2/CoO micromotors with a spherical Janus morphology and SEM image. Adapted with permission from ref. 48. Copyright 2020, American Chemical Society. (C) Core–shell silicon-based nanomotors and SEM image showing the silicon nanowire array, scale bar 10 µm. Reproduced from ref. 6 with permission from John Wiley and Sons, copyright 2017. (D) GaN/ZnO tubular micromotors and SEM image showing the tubular structure with different diameters. Reproduced from ref. 51 with permission from John Wiley and Sons, copyright 2019. (E) Schematic representation of a programmable micromotor based on a TiO_2/Si heterostructure.[11] (F) TiO_2/CdS micromotors and SEM image showing their a tubular structure. Reproduced from ref. 54 with permission from John Wiley and Sons, copyright 2021.

Another example of heterostructuring in micromachines is the development of core–shell nanomotors with a p-Si core and an n^+-Si shell using the vapor–liquid–solid growth method (Fig. 8(c)).[6] These silicon nanomotors were able to move under visible and near-infrared illumination at ultralow light intensity (approximately 3 mW cm^{-2}), making it a highly efficient device. Additionally, the motion trajectories of nanowires were altered by manipulating their end surface morphologies, resulting in various modes such as linear, circular, and rotational movements. By taking advantage of the strong optical resonance of the silicon nanowires, the spectral response of the nanomotors was also modulated by changing the diameter.

A less studied approach is the polarization of light to induce changes in the speed of the micro/nanomotors. In a recent study, a nanomotor made of core–shell Sb_2Se_3/ZnO nanowires with an anisotropic crystal structure was reported.[49] When illuminated with light polarized parallel to the nanowires, the nanomotor absorbs the light preferentially, resulting in an enhanced motion speed compared to perpendicular polarized light. By combining two of these nanomotors, a polarotactic artificial microswimmer was created, allowing navigation by controlling the polarization of the incident light. This dichroic microswimmer offers a significant reduction in required light intensity compared to previous methods, making it suitable for large-scale nanomanipulation and heat-sensitive applications.

The formation of n–n semiconductor heterojunctions offers an alternative approach to achieving charge separation in photoactive micromotors. This can be accomplished by creating a sharp junction between n-type semiconductors with different electron affinities.[50] One example of such a junction is the development of GaN/ZnO microtubes with a nanoarchitectured structure (Fig. 8(D)).[51] These microtubes were decorated with $(Ga_{1-x}Zn_x)(N_{1-x}O_x)$ nanowires on their surface, which greatly enhanced their stability and photocatalytic efficiency in the UV region. The unique nanoarchitecture of these micromotors resulted in enhanced propulsion. Moreover, the inclusion of ZnO enabled fluorescence emission when excited by UV light, making them suitable for imaging and tracking applications at the microscale.

On the other hand, programmable phototactic behaviors in light-driven nanomotors have also been achieved Si/TiO_2 Janus heterostructures (Fig. 8(E)).[11] These micromotors consist of a nanostructured photocathode and photoanode at opposite ends that release cations and anions, respectively, thereby propelling the microdevice *via* self-electrophoresis. By adjusting the zeta potential of the photoanode, the motion dynamics of the micromotor were manipulated to provide them with sensing capabilities of light stimuli, by either showing negative or positive phototaxis. This feature is commonly displayed by natural photosynthetic microorganisms, which are able to move towards the light for harvesting nutrients or away from it to avoid damage. Therefore, this innovative approach based on artificial phototactic micromotors offers a promising method for incorporating biomimetic features in artificial photoactive nanomotors.

CdS is a widely explored material in photocatalysis, due to its short bandgap and optimal redox band potential for hydrogen generation.[52,53] The coupling of this material with a wide bandgap photocatalyst is a common approach to avoid the photo-corrosion associated with sulfide-based semiconductors. In the field of photocatalytic micromotors, a heterojunction that might represent a *Z*-scheme heterostructure consists of the fabrication of TiO_2/CdS tubular micromotors able to move under visible-light irradiation in water (Fig. 8(F)).[54] To achieve this configuration, ZnO microrods were used as a sacrificial template. Moreover, the inclusion of magnetic nanoparticles enabled their external actuation under magnetic fields. Therefore, the use of semiconductor heterojunctions presents a promising approach to constructing efficient photocatalytic micromotors able to self-propel in pure water without requiring noble-metal components.

Overall, semiconductor–semiconductor heterojunctions offer several advantages in the design and functionality of heterostructured photocatalytic micromotors. Similar to metal–semiconductor heterojunctions, these types of micromotors can move under low light intensities and in pure water, making them versatile for various environmental conditions. Additionally, these heterojunctions also exhibit high motion

Open Access Article. Published on 14 June 2023. Downloaded on 1/14/2025 4:37:19 PM. This article is licensed under a Creative Commons Attribution-NonCommercial 3.0 Unported Licence.

efficiency and low recombination rates, ensuring reliable operation and enhanced functionality. However, there are certain disadvantages associated with semiconductor–semiconductor heterojunctions. Their fabrication often requires the use of templates and involves a multistep process, which can be complex and time-consuming. Moreover, sophisticated techniques are typically employed, adding to the complexity and cost of production.[55] Depending on the specific heterojunction, the reductive or oxidative potential of the single material may be reduced, which can impact its overall performance. To address these challenges, potential strategies include engineering the heterojunctions with appropriate valence and conduction bands to optimize their properties and facilitate charge transfer. Additionally, incorporating chemical wet methods in the synthesis process can contribute to reduce the fabrication cost and scalability.

Conclusions

In conclusion, this feature article has provided a comprehensive overview of the latest advancements in the field of photoactive micromotors based on metal-free and inorganic metal oxide-based semiconductors. We have highlighted the evolution from UV- to visible-light responsive photocatalytic micromotors, as well as advancements in the type of morphologies from simple amorphous particles to more sophisticated designs. We have also discussed the progression of photocatalytic micromotors from single component structures to multiple-component heterojunctions, which have improved the performance and capabilities of these micromotors. This article also emphasizes the significance of heterojunctions in the design of photoactive micromotors, as they allow for the integration of multiple materials with distinct properties. The various examples of heterojunctions presented in the article, including Si/TiO_2, TiO_2/Cu_2O, CoO/TiO_2, TiO_2/CdS, and GaN/ZnO, showcase the diverse range of configurations and possibilities of photoactive micromotors. Specifically, we have highlighted the potential for external control of motion behaviors by combining two types of semiconductors with different bandgaps, which enables control of the swimming direction (left and right) and/or motion modes under different wavelengths. Additionally, we have shown that the work function of metals in Janus photocatalytic micromotors can also influence their performance. Overall, these findings underscore the importance of a rational design approach that considers material properties such as bandgap, redox band potentials, Fermi levels, and stability. By optimizing the design of photocatalytic micromotors to minimize electron–hole pair recombination, we can fabricate devices with improved efficiency and performance.

The research discussed in this article has significant implications for various fields, including microfluidics, biomedical applications, and environmental remediation. In the latter, the potential for harvesting direct sunlight to induce the motion of photocatalytic micromotors is an attractive prospect for developing sustainable technology in water treatment. However, the high fabrication costs and the lack of in-depth studies on the reusability of such devices for meeting industrial requirements currently limit their applicability, rendering it in a very premature phase. Moreover, it is crucial to consider aspects, such as life-cycle assessment and stability of photocatalytic micromotors in future investigations.

Meanwhile, a more practical approach would involve integrating these photocatalytic micromotors into water treatment plants as a polishing step after tertiary treatment. Their inclusion in advanced oxidative processes would facilitate the treatment without requiring external mechanical agitation. In particular, the micromotors would contribute to effectively eliminate persistent or highly toxic contaminants that cannot be removed through common microbiological processes.

However, it is important to note that the applicability of these devices in real-world applications, particularly in non-transparent media and turbid environments, is currently not envisioned due to the limitations of light actuation. To fully unlock the potential of these devices in diverse applications, such as biomedicine and microbiology, it is necessary to develop photoactive micromotors able to store optical energy to have motion autonomy regardless of the swimming environment. Furthermore, developing near-infrared responsive micromotors and possibly coupling optical fibers to reach desired areas are viable options worth considering in the biomedical field.

As research in this field continues to advance, it is likely that we will see even more sophisticated and efficient photoactive micromotors in the future. Therefore, it is crucial to continue exploring these materials and their capabilities and to investigate their potential for integration into practical applications. We hope that this feature article serves as a valuable resource and inspires further research in this exciting and rapidly developing area of science.

Author contributions

K. V. contributed to conceptualization, formal analysis, funding acquisition, writing – original draft, and review & editing.

Conflicts of interest

There are no conflicts to declare.

Acknowledgements

K. V. acknowledges the support from the Spanish Ministry of Science (MCIN/AEI/10.13039/501100011033) and the European Union (Next generation EU/PRTR) through the Ramón y Cajal grant, RYC2021-031075-I and the MCIN/AEI/10.13039/501100011033 (CEX2019-000925-S). This research has also received funding from the European Research Council (ERC) under the European Union's Horizon 2020 research and innovation programme (GA no. 101076680; PhotoSwim).

References

1 L. Xu, F. Mou, H. Gong, M. Luo and J. Guan, *Chem. Soc. Rev.*, 2017, **46**, 6905–6926.

Open Access Article. Published on 14 June 2023. Downloaded on 1/14/2025 4:37:19 PM.
This article is licensed under a Creative Commons Attribution-NonCommercial 3.0 Unported Licence.

2 K. Villa and M. Pumera, *Chem. Soc. Rev.*, 2019, **48**, 4966–4978.

3 J. Wang, Z. Xiong, J. Zheng, X. Zhan and J. Tang, *Acc. Chem. Res.*, 2018, **51**, 1957–1965.

4 X. Xiong, X. Huang, Y. Liu, A. Feng, Z. Wang, X. Cheng, Z. He, S. Wang, J. Guo and X. Yan, *Chem. Eng. J.*, 2022, **445**, 136576.

5 R. Dong, Q. Zhang, W. Gao, A. Pei and B. Ren, *ACS Nano*, 2016, **10**, 839–844.

6 J. Wang, Z. Xiong, X. Zhan, B. Dai, J. Zheng, J. Liu and J. Tang, *Adv. Mater.*, 2017, **29**, 1701451.

7 K. Villa, C. L. Manzanares Palenzuela, Z. Sofer, S. Matějková and M. Pumera, *ACS Nano*, 2018, **12**, 12482–12491.

8 A. M. Pourrahimi, K. Villa, C. L. Manzanares Palenzuela, Y. Ying, Z. Sofer and M. Pumera, *Adv. Funct. Mater.*, 2019, **29**, 1808678.

9 K. Villa, F. Novotný, J. Zelenka, M. P. Browne, T. Ruml and M. Pumera, *ACS Nano*, 2019, **13**, 8135–8145.

10 X. Yuan, R. Ferrer-Campos, F. A. Garcés-Pineda and K. Villa, *Small*, 2023, **19**, 2207303.

11 B. Dai, J. Wang, Z. Xiong, X. Zhan, W. Dai, C.-C. Li, S.-P. Feng and J. Tang, *Nat. Nanotechnol.*, 2016, **11**, 1087–1092.

12 É. O'Neel-Judy, D. Nicholls, J. Castañeda and J. G. Gibbs, *Small*, 2018, **14**, 1801860.

13 D. Zhou, Y. C. Li, P. Xu, N. S. McCool, L. Li, W. Wang and T. E. Mallouk, *Nanoscale*, 2016, **9**, 75–78.

14 Q. Yang, H. Xu, H. Wen, H. Zhao, X. Liu, Y. Cai, H. Wang and R. Dong, *Appl. Mater. Today*, 2021, **22**, 100943.

15 M. Ibele, T. E. Mallouk and A. Sen, *Angew. Chem., Int. Ed.*, 2009, **48**, 3308–3312.

16 Y. Hong, M. Diaz, U. M. Córdova-Figueroa and A. Sen, *Adv. Funct. Mater.*, 2010, **20**, 1568–1576.

17 J. Palacci, S. Sacanna, A. Vatchinsky, P. M. Chaikin and D. J. Pine, *J. Am. Chem. Soc.*, 2013, **135**, 15978–15981.

18 C. Chen, F. Mou, L. Xu, S. Wang, J. Guan, Z. Feng, Q. Wang, L. Kong, W. Li, J. Wang and Q. Zhang, *Adv. Mater.*, 2017, **29**, 1603374.

19 Z. Ye, Y. Sun, H. Zhang, B. Song and B. Dong, *Nanoscale*, 2017, **9**, 18516–18522.

20 R. Dong, Y. Hu, Y. Wu, W. Gao, B. Ren, Q. Wang and Y. Cai, *J. Am. Chem. Soc.*, 2017, **139**, 1722–1725.

21 K. Villa, L. Děkanovský, J. Plutnar, J. Kosina and M. Pumera, *Adv. Funct. Mater.*, 2020, **30**, 2007073.

22 A. L. Stanford and J. M. Tanner, in *Physics for Students of Science and Engineering*, ed. A. L. Stanford and J. M. Tanner, Academic Press, 1985, pp.691–716.

23 K. Takanabe, *ACS Catal.*, 2017, **7**, 8006–8022.

24 D. Friedmann, C. Mendive and D. Bahnemann, *Appl. Catal., B*, 2010, **99**, 398–406.

25 J. Parmar, D. Vilela, K. Villa, J. Wang and S. Sánchez, *J. Am. Chem. Soc.*, 2018, **140**, 9317–9331.

26 V. Sridhar, F. Podjaski, Y. Alapan, J. Kröger, L. Grunenberg, V. Kishore, B. V. Lotsch and M. Sitti, *Sci. Robot.*, 2022, **7**, eabm1421.

27 V. Sridhar, F. Podjaski, J. Kröger, A. Jiménez-Solano, B.-W. Park, B. V. Lotsch and M. Sitti, *Proc. Natl. Acad. Sci. U. S. A.*, 2020, **117**, 24748–24756.

28 K. Villa, J. Vyskočil, Y. Ying, J. Zelenka and M. Pumera, *Chem. – Eur. J.*, 2020, **26**, 3039–3043.

29 M. Wittmann, S. Heckel, F. Wurl, Z. Xiao, T. Gemming, T. Strassner and J. Simmchen, *Chem. Commun.*, 2022, **58**, 4052–4055.

30 W. Liu, X. Chen, X. Lu, J. Wang, Y. Zhang and Z. Gu, *Adv. Funct. Mater.*, 2020, **30**, 2003195.

31 S. Heckel, C. Bilsing, M. Wittmann, T. Gemming, L. Büttner, J. Czarske and J. Simmchen, *Adv. Sci.*, 2022, **9**, 2105009.

32 W. Liu, X. Chen, X. Ding, Q. Long, X. Lu, Q. Wang and Z. Gu, *Nanoscale Horiz.*, 2021, **6**, 238–244.

33 V. Chakrapani, in *Encyclopedia of Applied Electrochemistry*, ed. G. Kreysa, K. Ota and R. F. Savinell, Springer, New York, NY, 2014, pp.1882–1893.

34 G. Shao, *Energy Environ. Mater.*, 2021, **4**, 273–276.

35 X. Wang, V. Sridhar, S. Guo, N. Talebi, A. Miguel-López, K. Hahn, P. A. van Aken and S. Sánchez, *Adv. Funct. Mater.*, 2018, **28**, 1705862.

36 D. Zhou, Y. C. Li, P. Xu, L. Ren, G. Zhang, T. E. Mallouk and L. Li, *Nanoscale*, 2017, **9**, 11434–11438.

37 D. Zhou, L. Ren, Y. C. Li, P. Xu, Y. Gao, G. Zhang, W. Wang, T. E. Mallouk and L. Li, *Chem. Commun.*, 2017, **53**, 11465–11468.

38 X. Wang, L. Baraban, V. R. Misko, F. Nori, T. Huang, G. Cuniberti, J. Fassbender and D. Makarov, *Small*, 2018, **14**, 1802537.

39 F. Mou, L. Kong, C. Chen, Z. Chen, L. Xu and J. Guan, *Nanoscale*, 2016, **8**, 4976–4983.

40 L. Wang, M. N. Popescu, F. Stavale, A. Ali, T. Gemming and J. Simmchen, *Soft Matter*, 2018, **14**, 6969–6973.

41 F. Mushtaq, A. Asani, M. Hoop, X.-Z. Chen, D. Ahmed, B. J. Nelson and S. Pané, *Adv. Funct. Mater.*, 2016, **26**, 6995–7002.

42 Q. Wang, C. Wang, R. Dong, Q. Pang and Y. Cai, *Inorg. Chem. Commun.*, 2018, **91**, 1–4.

43 S. Hoang and P.-X. Gao, *Adv. Energy Mater.*, 2016, **6**, 1600683.

44 P. Zhou, J. Yu and M. Jaroniec, *Adv. Mater.*, 2014, **26**, 4920–4935.

45 X. Huang, J. Wang, T. Li, J. Wang, M. Xu, W. Yu, A. E. Abed and X. Zhang, *Beilstein J. Nanotechnol.*, 2018, **9**, 30–41.

46 S. Chen, T. Takata and K. Domen, *Nat. Rev. Mater.*, 2017, **2**, 1–17.

47 Y. Sasaki, H. Nemoto, K. Saito and A. Kudo, *J. Phys. Chem. C*, 2009, **113**, 17536–17542.

48 V. Sridhar, B.-W. Park, S. Guo, P. A. van Aken and M. Sitti, *ACS Appl. Mater. Interfaces*, 2020, **12**, 24149–24155.

49 X. Zhan, J. Zheng, Y. Zhao, B. Zhu, R. Cheng, J. Wang, J. Liu, J. Tang and J. Tang, *Adv. Mater.*, 2019, **31**, 1903329.

50 W. G. Oldham and A. G. Milnes, *Solid-State Electron.*, 1963, **6**, 121–132.

51 N. Wolff, V. Ciobanu, M. Enachi, M. Kamp, T. Braniste, V. Duppel, S. Shree, S. Raevschi, M. Medina-Sánchez, R. Adelung, O. G. Schmidt, L. Kienle and I. Tiginyanu, *Small*, 2020, **16**, 1905141.

52 K. Villa, X. Domènech, U. M. García-Pérez and J. Peral, *Catal. Lett.*, 2016, **146**, 100–108.

53 K. Villa, X. Domènech, U. M. García-Pérez and J. Peral, *RSC Adv.*, 2016, **6**, 36681–36688.

54 Y. Ying, J. Plutnar and M. Pumera, *Small*, 2021, **17**, 2100294.

55 Y. Zheng, H. Zhao, Y. Cai, B. Jurado-Sánchez and R. Dong, *Nano-Micro Lett.*, 2022, **15**, 20.